Palaeogeography, Palaeoclimatology, Palaeoecology 625 (2023) 111680

Contents lists available at ScienceDirect

Palaeogeography, Palaeoclimatology, Palaeoecology

journal homepage: www.elsevier.com/locate/palaeo

Carbonate factories and their critical control on the geometry of carbonate platforms (mid-Cretaceous, southern Iran)

Yiwei Xu [a,b], Xiumian Hu [b,*], Eduardo Garzanti [c], Gaoyuan Sun [d], Jingxin Jiang [b], Juan Li [a], Shijie Zhang [e], Felix Schlagintweit [f], Xin Rao [a]

[a] State Key Laboratory of Palaeobiology and Stratigraphy, Nanjing Institute of Geology and Palaeontology and Center for Excellence in Life and Paleoenvironment, Chinese Academy of Sciences, Nanjing 210008, China
[b] State Key Laboratory of Mineral Deposits Research, School of Earth Sciences and Engineering, Nanjing University, Nanjing 210023, China
[c] Department of Earth and Environmental Sciences, Università di Milano-Bicocca, Milano 20126, Italy
[d] College of Oceanography, Hohai University, Nanjing 210098, China
[e] College of Tourism, Henan Normal University, Xinxiang 453000, China
[f] Lerchenauer str. 167, Munich, 80935, Germany

ARTICLE INFO

Editor: A Dickson

Keywords:
Carbonate platform
Platform geometry
Microfacies
Carbonate factory
Mid-Cretaceous
Iran

ABSTRACT

Tropical rimmed platforms represent a much more efficient protection from coastal erosion than carbonate ramps. Understanding the controlling factors of platform geometry is therefore crucial to predict the fate of rimmed platforms under global-warming conditions. Here, we present detailed biostratigraphic, sedimentological, geochemical, and high-resolution carbon-isotope analyses of mid-Cretaceous (Albian-Cenomanian) carbonate rocks well exposed in the Khormoj section located in the Zagros Mountains of southern Iran. Sixteen microfacies were identified, allowing us to define the superposition of different platform geometries, a carbonate ramp in the Albian and a rimmed platform in the Cenomanian. Biostratigraphic and carbon-isotope analyses allowed us to identify the OAE1b, OAE1d, and Middle Cenomanian events in the Khormoj section. The paleodepth changes documented by carbonate microfacies testify to two transgressive events that can be correlated with long-term eustatic curves during the ramp stage. The Albian ramp was formed by orbitolinids under high siliciclastic input whereas the Cenomanian rimmed platform was built by rudists during clear water conditions. These two carbonate factories have drastic different carbonate sedimentation modes. The orbitolinid factory is characterized by a low carbonate production rate and fine carbonate grains resulting in ramp geometry, whereas the rudist factory is characterized by a high carbonate production rate and coarse carbonate grains leading to a rimmed platform geometry.

1. Introduction

Modern tropical platform carbonates are mostly rimmed by reefs built by hermatypic corals (e.g., Bahamas or Great Barrier Reef; Schlager, 2005; Jones, 2010; Reijmer, 2021). The reef at the rimmed platform margin serves as a barrier that drastically reduces wave energy (e.g., by 97%), thus providing an efficient protection against coastal erosion in regions populated by ~200 million people worldwide (Ferrario et al., 2014).

However, rimmed platforms are only one type of carbonate platform. A very different type is homoclinal ramps that lack any slope-break (Pomar, 2001; Flügel, 2010) and thus do not offer an effective coastal protection. The key difference between these two end member is their depositional geometry, which is controlled by the ratio between carbonate production and accumulation, influenced in turn by temperature (Pomar, 2001; Schlager, 2005), relative sea-level change (Williams et al., 2011), trophic level (Mutti and Hallock, 2003), siliciclastic input (Pomar and Haq, 2016), and other factors (Sultana et al., 2022).

The geometry of carbonate platforms grown along the Arabian passive continental margin changed repeatedly from ramp to rimmed during the mid-Cretaceous (van Buchem et al., 2002, 2011; Droste, 2010; Razin et al., 2010). Third-order relative sea-level changes have been proposed as one mainly controlling factors while ramps and rimmed platforms forming during transgression and highstand stages,

* Corresponding author.
E-mail address: huxm@nju.edu.cn (X. Hu).

https://doi.org/10.1016/j.palaeo.2023.111680
Received 21 February 2023; Received in revised form 14 May 2023; Accepted 7 June 2023
Available online 10 June 2023

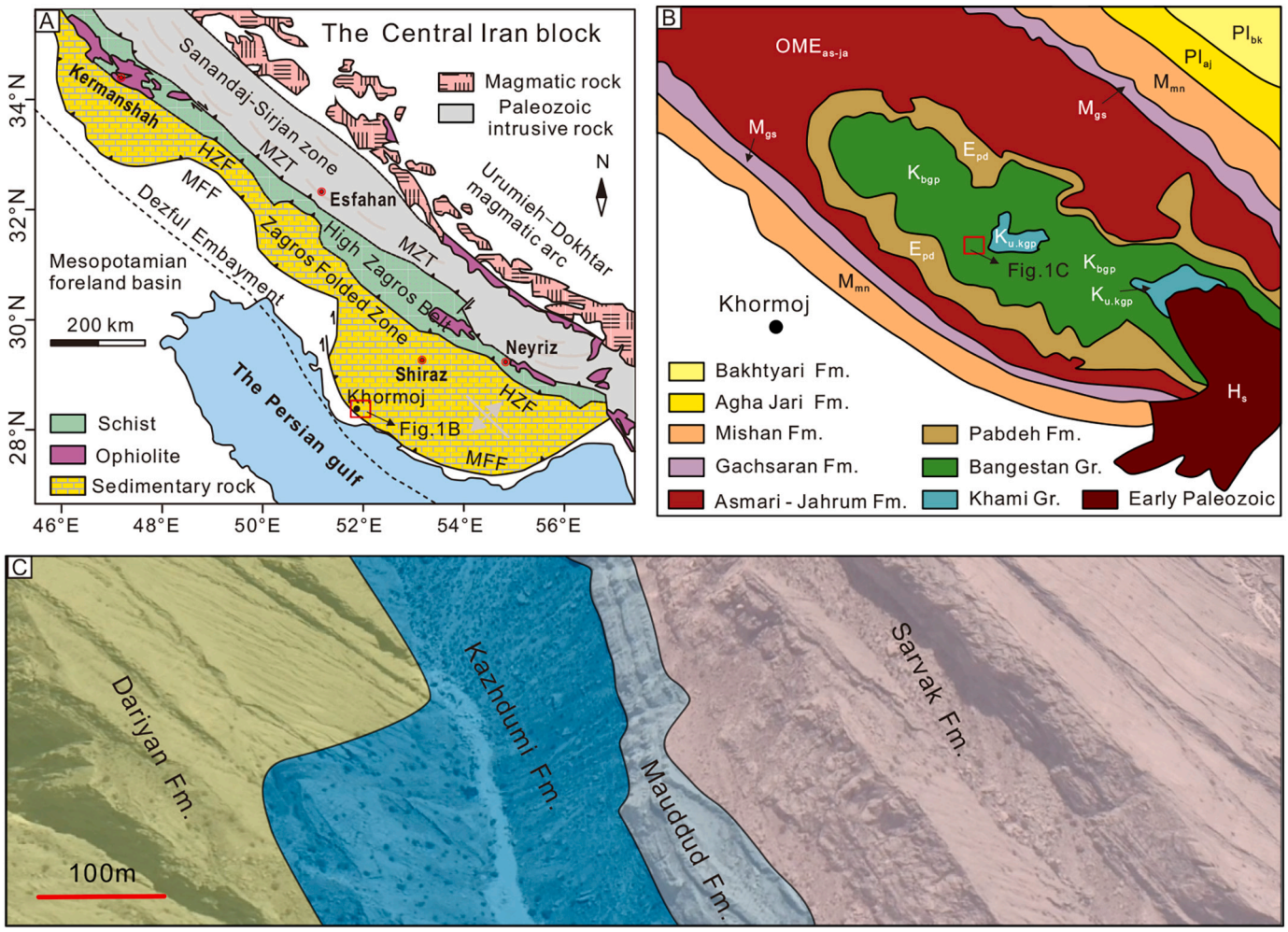

Fig. 1. Geology of the study area. (A) Simplified tectonic map of southern Iran (redrawn from Homke et al., 2009). MZT: Main Zagros Thrust; HZF: High Zagros Fault; MFF: Mountain Front Fault. (B) Geological map of the Khormoj area (redrawn from the 1:250,000 map). (C) Studied Khormoj stratigraphic section.

respectively (Razin et al., 2010). How short-term sea-level changes influence the relationship between carbonate production and accumulation? The other factors that potentially influence such a relationship need to be fully investigated in order to improve on our knowledge of the relative role played by several interacting controls and thus predict the response of carbonate platforms to accelerated global warming.

Mid-Cretaceous carbonate successions accumulated at low latitudes along the Arabian southern margin of Neotethys are spectacularly exposed in the Zagros fold-belt of southern Iran. In this article, we present a biostratigraphic, sedimentological, elemental-geochemistry, and high-resolution carbon-isotope study of Albian-Cenomanian carbonate strata exposed in the Khormoj section in southern Iran. Our principal aim is to investigate the processes that controlled the change in platform geometry through time.

2. Geological setting

The Zagros fold-thrust belt, extending from SE Turkey to S Iran (Fig. 1A), consists of four NW-SE–trending sub-parallel structural domains (from NE to SW): the Sanandaj-Sirjan zone, the High Zagros belt, the Zagros folded zone, and the Mesopotamian–Persian Gulf foreland basin (Homke et al., 2009). The studied area, belonging to the Zagros folded zone (Fig. 1B), was part of the southern passive margin of the Neo-Tethys Ocean, where carbonate-dominated strata accumulated during the mid-Cretaceous in tropical platforms including several intra-shelf basins (Ziegler, 2001; Alavi, 2004). A major geodynamic change took place by the late Cenomanian, when the passive-margin succession recorded ophiolite obduction eventually followed by Cenozoic collision with the Central Iranian block (Alavi, 2004; Allen and Armstrong, 2008; Saura et al., 2015).

The measured section exposing Aptian to Cenomanian strata (Dayrian, Kazhdumi, Mauddud and Sarvak formations) is located to the northwest of the Persian Gulf (Fig. 1A). A previous sedimentological study of this succession was reported by van Buchem et al. (2010) and Vincent et al. (2015). The Kazhdumi Formation was assigned to the early-middle Albian based on two ammonite species collected from the lower part of the unit. In the absence of biostratigraphic evidence, a late Albian age was assigned to the Mauddud Formation based on sequence stratigraphy (Vincent et al., 2015) and the Sarvak Formation was assigned to the Cenomanian based on carbon-isotope correlation (Vincent et al., 2015).

The Kazhdumi and Mauddud formations are described as carbonate ramps (Razin et al., 2010; van Buchem et al., 2011; Vincent et al., 2015), whereas the Sarvak Formation has been considered either a rimmed platform based mainly on field observations (Razin et al. (2010) and Vincent et al. (2015)) or a carbonate ramp or shelf mostly based on microfacies analysis (Ghabeishavi et al., 2010; Mehrabi and Rahimpour-Bonab, 2014; Esrafili-Dizaji et al., 2015; Rikhtegarzadeh et al., 2017; Mohajer et al., 2022).

Fig. 2. Outcrop photographs. (A) Burgan ironstone and its stratigraphic boundaries with underlying Dariyan and overlying Kazhdumi fms.; (B) Closer view of boundary between Dariyan Fm. and Burgan ironstone; (C) Closer view of boundary between Burgan ironstone and Kazhdumi Fm.; (D) Nodular limestone in Kazhdumi Fm.; (E) Conformable contact between Kazhdumi and Maudud fms.; (F) Sarvak Fm.; (G) Large-scale cross bedding in lower part of Sarvak Fm.; (H) Prograding clinoforms in Sarvak Fm.; (I) Limestone-marlstone alternations in middle part of Sarvak Fm.; (J) Intensely bioturbated marlstone interstratified with an erosive based limestone bed.

3. Methods

3.1. Samples and microfacies analysis

The Khormoj section is exposed to the northeast of Khormoj city (N 28°41′45.3″; E 51°26′58.4″, Fig. 1A) along the flanks of an anticline including Jurassic (Khami Group), Cretaceous (Bangestan Group) and Cenozoic (Pabdeh, Asmari, Jahrum, Gachsaran, Mishan, Agha Jari, and Bakhtyari formations) strata (Fig. 1B). This study focuses on the Kazhdumi, Maudud, and Sarvak formations of the Bangestan Group (Fig. 1C). Samples were collected with an average spacing of 1–2 m. A total of 171 thin sections were used for microfacies analysis, based on grain components, textures, and fossil assemblages. Carbonate rocks were classified after Dunham (1962) integrated by Embry and Klovan (1971).

3.2. Carbon and oxygen stable isotopes geochemistry

The analysis of carbon and oxygen isotopes in bulk samples were performed at the State Key Laboratory for Mineral Deposits Research at

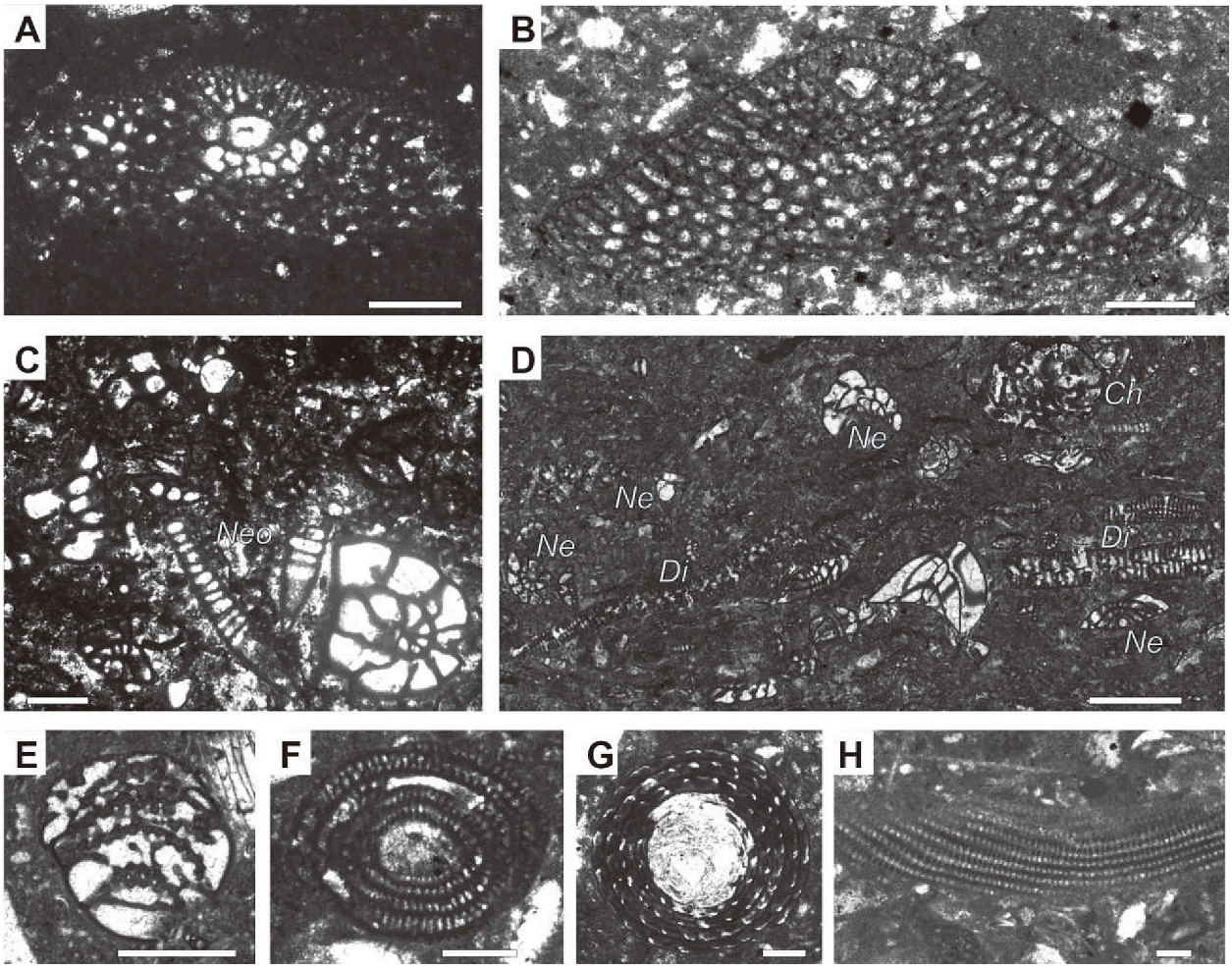

Fig. 3. Larger benthic foraminifers from the Khormoj section. (A) *Mesorbitolina texana* (Roemer).19KJ 69; (B) *Orbitolina* cf. *sefini* Henson. 19KJ106; (C) Nezzazatids and two specimens of *Neodubrovnikella turonica* (Said and Kenawy) (Ne). 19KJ159. (D) Assemblage of *Nezzazata* div. sp. (Ne) and *Dicyclina* sp. (Di). 19KJ159. (E) *Chrysalidina* cf. *gradata* Orbigny. 19KJ160. (F) *Ovalveolina* cf. *crassa* De. Sample Castro. 19KJ 165. (G) *Decastroia* sp. Sample 19KJ 166. (H) *Pastrikella* sp. 19KJ 165.

Nanjing University using an in-line GasBench II auto sampler coupled to a Thermo Finnigan MAT Delta Plus XP mass spectrometer. Powdered samples were obtained by micro-drilling, taking care to avoid cement-filled veins, pores and bioclasts, and reacted with purified orthophosphoric acid at 70 °C. Isotopic measurements were calibrated to Chinese national standard calcium carbonate sample GBW04405 ($\delta^{13}C_{VPDB}$ 0.57‰ ± 0.03‰; $\delta^{18}O_{VPDB}$ -8.49‰ ± 0.14‰). Isotope ratios are expressed in standard delta notation (δ) as per mil deviations relative to the Vienna Pee Dee Belemnite (VPDB) standard. Analytical precision (1σ) was better than 0.1‰ for $\delta^{13}C$ and than 0.05‰ based on duplicate measurements of standards and samples. Geochemical data for carbon and oxygen isotopes are provided in Table S1.

3.3. Element geochemistry of carbonate

About 50 mg of powdered samples of shallow-water carbonate rocks were weighed and left to dissolve overnight in 3 ml of distilled 0.5 M acetic acid. The solutions were centrifuged, and the supernatant transferred to another beaker. The residual noncarbonate impurities were rinsed three times using ultrapure water and the solutions were added to the previous supernatant. The leachates were converted to a nitric acid medium, used for elemental analysis carried out at NIGPAS. Trace-element concentrations were determined using an Agilent 7700A inductively-coupled-plasma mass-spectrometer (ICP-MS) with analytical precision better than ±2%. Major elements were measured using an Agilent 710 ICP-OES with analytical precision better than ±5%. Geochemical data for carbonate phase and percentages of the siliciclastic fraction are provided in Tables S2.

4. Results

4.1. Stratigraphy

The Albian to Cenomanian succession exposed in the Khormoj section consists, from bottom to top, of the Kazhdumi, Mauddud, and Sarvak formations (Fig. 1C). The ~6 m base of the Kazhdumi Formation, separated from the underlying Dariyan Formation by a paleosoil bed (Fig. 2A, B), consists of ferriferous arenite (Burgan Ironstone) correlated with the deltaic Burgan Sandstone in Arabia (Ziegler, 2001; Vincent et al., 2015; Mehrabi et al., 2019; Fig. 2C). The Burgan ironstone is overlain by ~95 m of nodular limestone locally rich in orbitolinids (Fig. 2D). The ~70 m-thick Mauddud Formation consists of thick-bedded bioclastic limestone (Fig. 2E). The Sarvak Formation (~ 217 m-thick) can be subdivided into four members; member 1 consists of ~37 m-thick poorly exposed marlstone (Fig. 2F); member 2 by ~90 m-thick massive rudist grainstone with cross bedding (Fig. 2G) and is onlapped by member 3, represented by thin-bedded limestone followed by ~60 m of alternating limestone and marlstone (Fig. 2H, I). The ~30-m-thick member 4 consists of rudist-rich limestone with prograding clinoforms (Fig. 2H).

Age constraints are provided by the larger benthic foraminifers identified in this study, including *Mesorbitolina texana* (Roemer) and

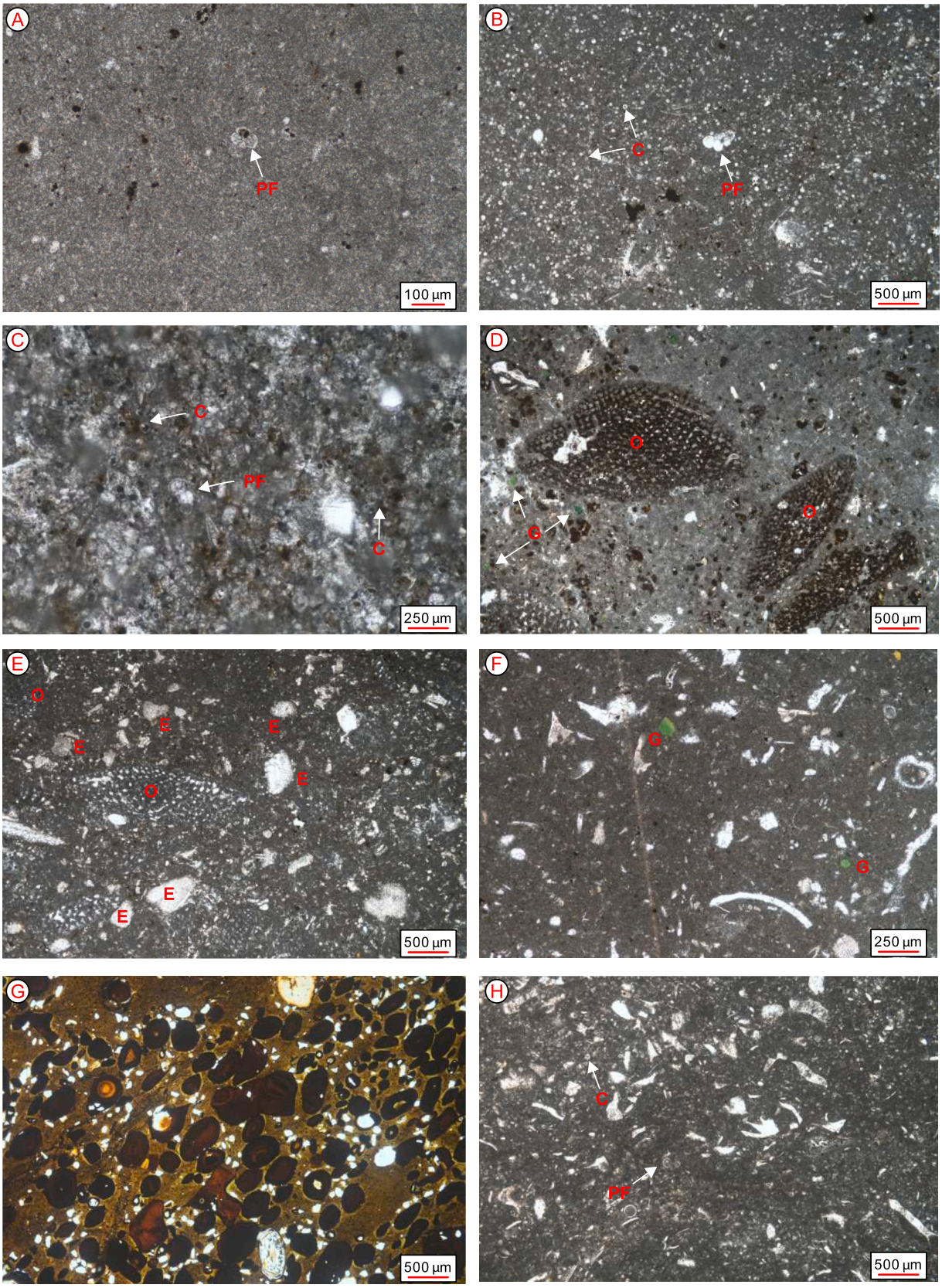

Fig. 4. Representative microfacies from the Khormoj section. (A) MF1 Mudstone with planktonic foraminifers (19KJ115); (B) MF2 Calcisphere wackestone with planktonic foraminifers (19KJ183); (C) MF3 Calcisphere packstone (19 KJ177); (D) MF4 Orbitolinid wackestone (19 KJ65); (E) MF5 Orbitolinid-echinoderm wackestone (19 KJ58); (F) MF6 Bioclastic wackestone (19KJ55); (G) MF7 Oolitic ironstone with sparse quartz grains (19KJ37); (H) MF8 Fine bioclastic wackestone-packstone with calcispheres (19KJ182); PF-Planktonic foraminifer, C-Calcisphere, O-Orbitolinid, G-Glaucony, E-Echinoderm.

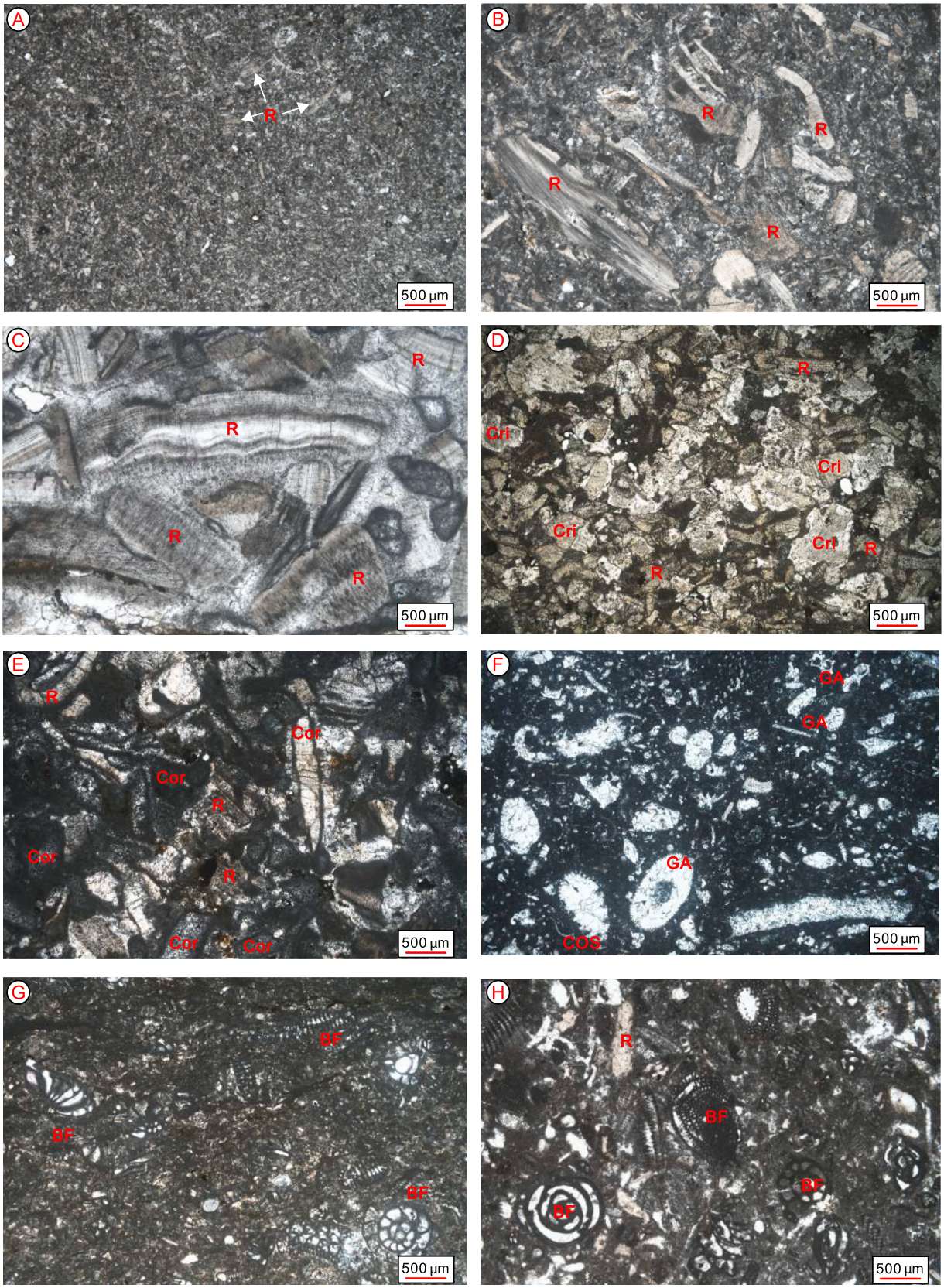

Fig. 5. Representative microfacies from the Khormoj section. (A) MF9 Rudist wackestone-packstone (19KJ195); (B) MF10 Rudist floatstone (19KJ204); (C) MF11 Rudist rudstone (19KJ215); (D) MF12 Echinoderm-rudist packstone-grainstone (19KJ125); (E) MF13 Cortoid packstone-grainstone (19KJ152); (F) MF14 Green algae wackestone with small benthic foraminifer (19KJ95); (G) MF15 Bioclastic wackestone with benthic foraminifers (19KJ159); (H) MF16 Benthic foraminifer wackestone (19KJ165); R-Rudist, Cri-Crinoid, Cor-Cortoid, GA-Green algae, BF-Benthic foraminifer. (For interpretation of the references to colour in this figure legend, the reader is referred to the web version of this article.)

Orbitolina cf. *sefini* Henson in the middle and upper parts of the Kazhdumi Formation (Fig.3 A, B). Early Albian and late Albian ages are thus indicated for the lower and middle part of the Kazhdumi Formation (Schroeder and Neumann, 1985; Simmons et al., 2000). Limestones in the middle part of the Sarvak Formation yielded *Neodubrovnikella turonica* (Said and Kenawy), *Nezzazata* div. sp., *Chrysalidina* cf. *gradate* Orbigny, *Ovalveolina* cf. *crassa* De Castro, *Decastroia* sp., and *Pastrikella* sp. (Fig. 3 C, D, E and F), indicating the middle Cenomanian (Schroeder and Neumann, 1985).

4.2. Carbonate microfacies

Based on field observations, textural features and fossil assemblages, 16 microfacies (MF1 to MF16) were distinguished in the Khormoj section, identifying seven sedimentary facies.

Basin to toe of slope

MF1 Mudstone with planktonic foraminifers

Thin-bedded limestones of the lowermost Sarvak Formation are mudstones with a few planktonic foraminifers (Fig. 4A), indicating a low-energy pelagic environment (Flügel, 2010).

MF2 Calcisphere wackestone with planktonic foraminifers

Thin marls in the middle Sarvak Formation contain calcispheres and a few non-keeled planktonic foraminifers, small bioclasts and sponge spicules (Fig. 4B). Bioclasts set in micritic matrix account for ~30% of the rock. Calcispheres and non-keeled planktonic foraminifers indicate a basinal environment with paleowater depths of 50–100 m, consistent with previous estimates (80–90 m) based on downlap geometries (Vincent et al., 2015).

MF3 Calcisphere packstone

In the Khormoj section, burrowed packstones with calcispheres and planktonic foraminifers represent 50–60% of the rock (Fig. 4C) and are associated with sparse echinoderms, bivalves, sponge spicules and other bioclasts (2–7%). MF3 alternates with MF2 with a sharp erosive base (Fig. 2I and J). The high density of planktonic tests suggests hydraulic sorting during transport by gravity flow, the interbedded MF2 to MF3 representing the background pelagic environment. The grain-supported texture together with the presence of shallow-water bioclasts and extensive bioturbation also suggest deposition by turbiditic currents or storms, supplying nutrients and oxygen to the toe of the carbonate slope.

Open marine

MF4 Orbitolinid wackestone-marlstone

Thin-bedded to nodular limestones of the Kazhdumi Formation (Fig. 4D) contain Discoidal orbitolinids representing 8–10% of the rock and set in micritic matrix. Bivalves, ostracods, gastropods, small benthic foraminifers, and other bioclasts are minor (3–5%). Glaucony grains are rare. Discoidal orbitolinids prevail over conical forms in scarcely illuminated deeper-water environments (Vilas et al., 1995). Glaucony suggests sediment starvation during sea-level rise (Garzanti, 1991; Flügel, 2010; Fürsich et al., 2021). A low-energy open-marine environment below fair-weather wave base is indicated.

MF5 Orbitolinid-echinoderm wackestone

Matrix-supported nodular limestones in the Kazhdumi Formation contain both orbitolinids (3–7%) and echinoderms (3–5%) (Fig. 4E), associated with sparse bivalves, gastropods, ostracods, and planktonic foraminifers. The close association with MF4 indicates an open-marine environment below fair-weather wave base.

MF6 Bioclastic wackestone

Abundant bioclasts set in micritic matrix include bivalves, green algae, gastropods, echinoderms, ostracods, small benthic foraminifers, orbitolinids, and serpulids (Fig. 4F). Small rotaliina and glaucony grains are rare. The decreased content of discoidal orbitolinids and association with MF5 and MF14 indicates an open marine environment with water depth shallower than MF5 but deeper than MF14.

MF7 Oolitic ironstone with quartz grains

Ferriferous arenites at the base of the Kazhdumi Formation consist of sideritic ooids and intraclasts with quartz grains set in sideritic cement (Fig. 4G). The sideritic intraclasts and cement imply an in situ origin. Authigenic siderite may form during transgressions in starved tropical delta-front or prodelta settings (Mehrabi et al., 2019; Fürsich et al., 2021). Extensive bioturbation and siderite growth indicate sub-oxic conditions. The broken ooids and intraclasts point at turbulent transport during storm events. An open-marine environment is indicated, below fair-weather wave base but shallower than the directly overlying MF4.

Slope

MF8 Fine bioclastic wackestone-packstone with calcispheres

Calcispheres set in micritic matrix are associated with small bioclasts including echinoderm plates and planktonic foraminifers (Fig. 4H). The association with MF3 (containing less benthic fossils) and MF9 indicates lower-slope to toe-of-slope environments.

MF9 Rudist wackestone-packstone

Abundant fine rudist debris, representing 40–70% of the rock and associated with minor echinoderms and other bioclasts, are set in micritic matrix (Fig. 5A). Planktonic foraminifers and micritic envelopes are mostly lacking. Associated with MF8 and MF10, together with field relationships, indicate the bottomsets of prograding platform-margin clinoforms (Fig. 2H).

MF10 Rudist floatstone

Abundant rudist debris represents 35–75% of the rock (Fig. 5B). Echinoderms are rare. Bimodal size distribution with coarser rudist clasts floating in the matrix of fine rudist debris points at gravity flow deposits. Association with MF9 and MF11, and occurrence in the upper part of the prograding platform margin indicate slope environments dominated by gravity flows.

Rudist shoal

MF11 Rudist grainstone-rudstone

Coarse rudist debris (3–5 mm) cemented by sparite (Fig. 5C) represents 60–80% of the rock. Peloids and small benthic foraminifers are minor. Lack of micrite indicates a high-energy shoal environment.

MF12 Crinoids-rudist packstone

Thick-bedded limestones in the middle part of the Sarvak Formation contain grain-supported, well sorted rudist debris (15%–40%; average size 0.2–0.3 mm) and crinoids (20%–35%) (Fig. 5D). Intraclasts are rare. MF12 directedly overlies MF11 in the lower part of the Sarvak Formation and large-scale cross bedding (Fig. 2G) indicate a near shoal environment.

MF13 Cortoid grainstone

Bivalve and other shell debris with constructive micritic envelopes indicating firmgrounds to hardgrounds (Ge et al., 2020) are cemented by sparite (Fig. 5E). Intraclasts are minor. Well sorted cortoids (average size 0.5–1 mm) and lack of micrite indicate a shoal environment with low accumulation rate (Flügel, 2010).

Shallow neritic sea

MF14 Green algae wackestone with small benthic foraminifers

Thick-bedded limestones in the Mauddud Formation are dominated by trocholinids, *Coscinoconus*, and green algae set in micritic matrix (Fig. 5F). Green algae (e.g., *Permocalculus* and *Dasycladale*) and benthic foraminifera (e.g., trocholinids and *Coscinoconus*) represent 5–20% of the rock, 3–8% being accounted for by bivalves, conical orbitolinids, other small benthic foraminifers, echinoderms, and gastropods. Green algae indicate the euphotic zone and dasycladaceans are restricted to water depths of a few meters (Flügel, 2010). Trocholinids thrive in a shallow subtidal environment (Hosseini et al., 2021). Deposition took place in a low-energy neritic environment shallower than for associated MF4 and MF5.

Lagoon

MF15 Bioclastic wackestone with benthic foraminifers

Thin-bedded limestones in the middle part of the Sarvak Formation are dominated by benthic foraminifers (miliolids, alveolininds, and others) representing 5–20% of the rock (Fig. 5G). Minor green algae, bivalves, and echinoderms also occur. The faunal assemblage indicates a shallow lagoon with water depths ≤10 m (Davies et al., 2002;

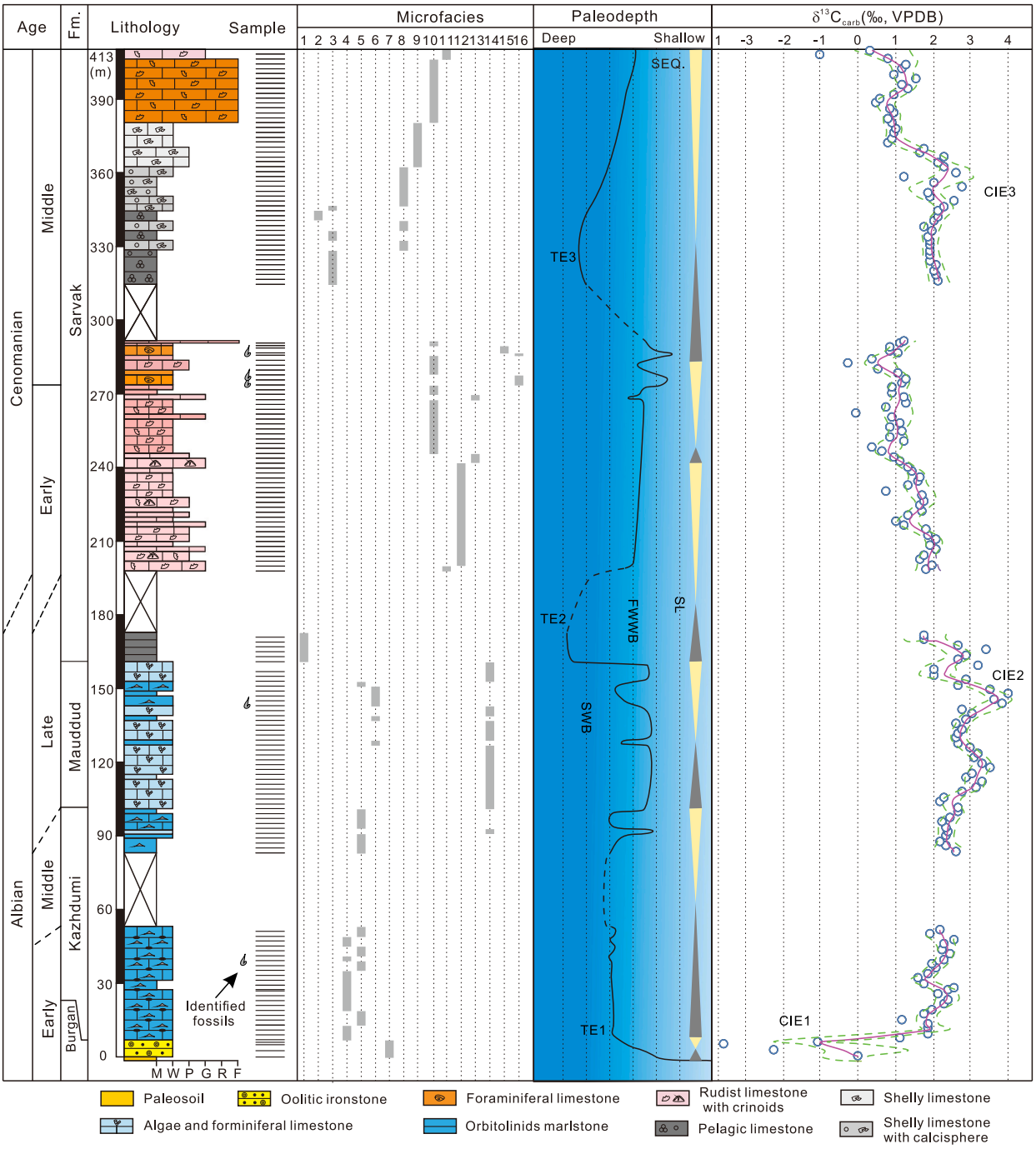

Fig. 6. Stratigraphic log of the Khormoj section showing identified microfacies, reconstructed paleodepth curve and whole-rock carbonate $\delta^{13}C$. Triangles represent third-order sequences recognized by Vincent et al. (2015). SL: Sea level; FWWB: Fair weather wave base, SWB: Storm wave base. TE: Transgressive event; SEQ.: Sequences; CIE: carbon-isotope excursion; VPDB: Vienna Pee Dee Belemnite.

Ghabeishavi et al., 2010).

MF16 Wackestone with benthic foraminifers

Abundant benthic foraminifers (mainly miliolids, alveolinids, nezzazatids, dicyclinids) set in micritic matrix (Fig. 5H) represent 10–15% of the rock, associated with minor bivalves, green algae, and other bioclasts (2–7%). MF16 onlaps onto MF12 (Fig. 2H). Abundant miliolids and micrite indicate a low-energy backshoal lagoon (Flügel, 2010).

4.3. *Platform evolution and depositional model*

The reconstructed paleodepth curve for the mid-Cretaceous succession exposed in the Khormoj section shows an overall deepening trend punctuated by three major transgressive episodes. The first transgression (TE1) is documented by the Burgan oolitic ironstone (MF7) at the base of the Kazhdumi Formation, passing upwards to orbitolinid wackestone (MF4, Fig. 6). The middle and upper parts of the Kazhdumi Formation are dominated by MF4 and MF5 deposited in an open marine environment. The Mauddud Formation mainly testifies a shallower marine environment (MF14) with three episodes of open-marine deposition testified by MF5 and MF6. At the top of the Mauddud Formation, the change from MF14 to MF1 documents the TE2 event. The lower Sarvak Formation records a shallowing-upward trend from basinal (MF1) to shoal environments (MF11–13, Fig.6). The upper part of the Sarvak Formation records the TE3 event, when the rudist shoal was

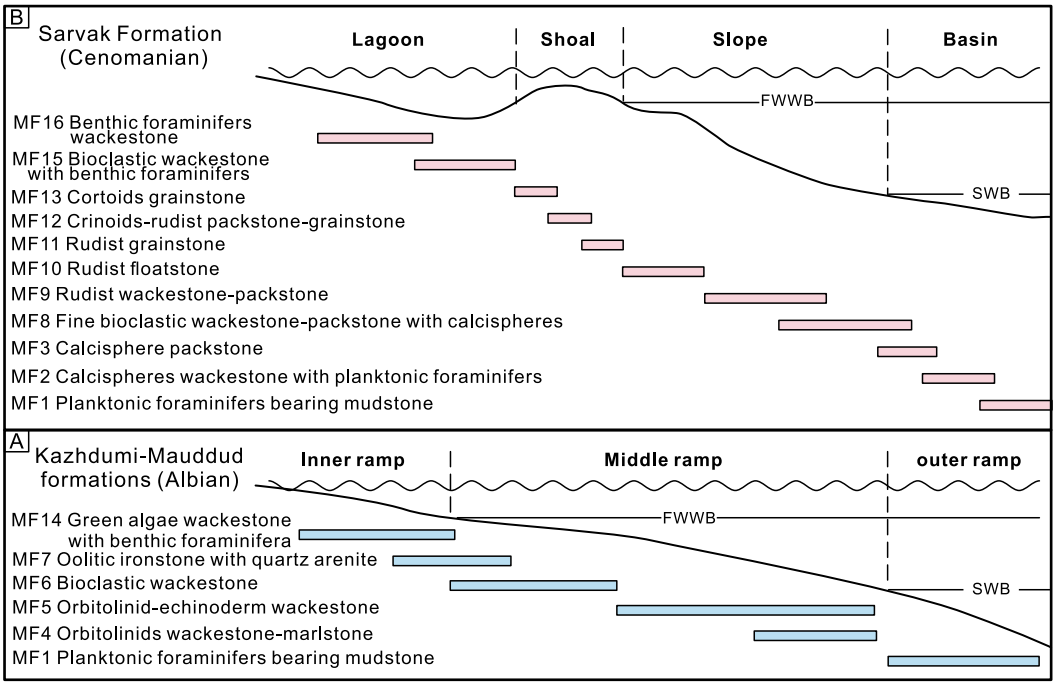

Fig. 7. Depositional model (A) Kazhdumi and Mauddud formations. (B) Sarvak Formation. FWWB: Fair weather wave base, SWB: Storm wave base.

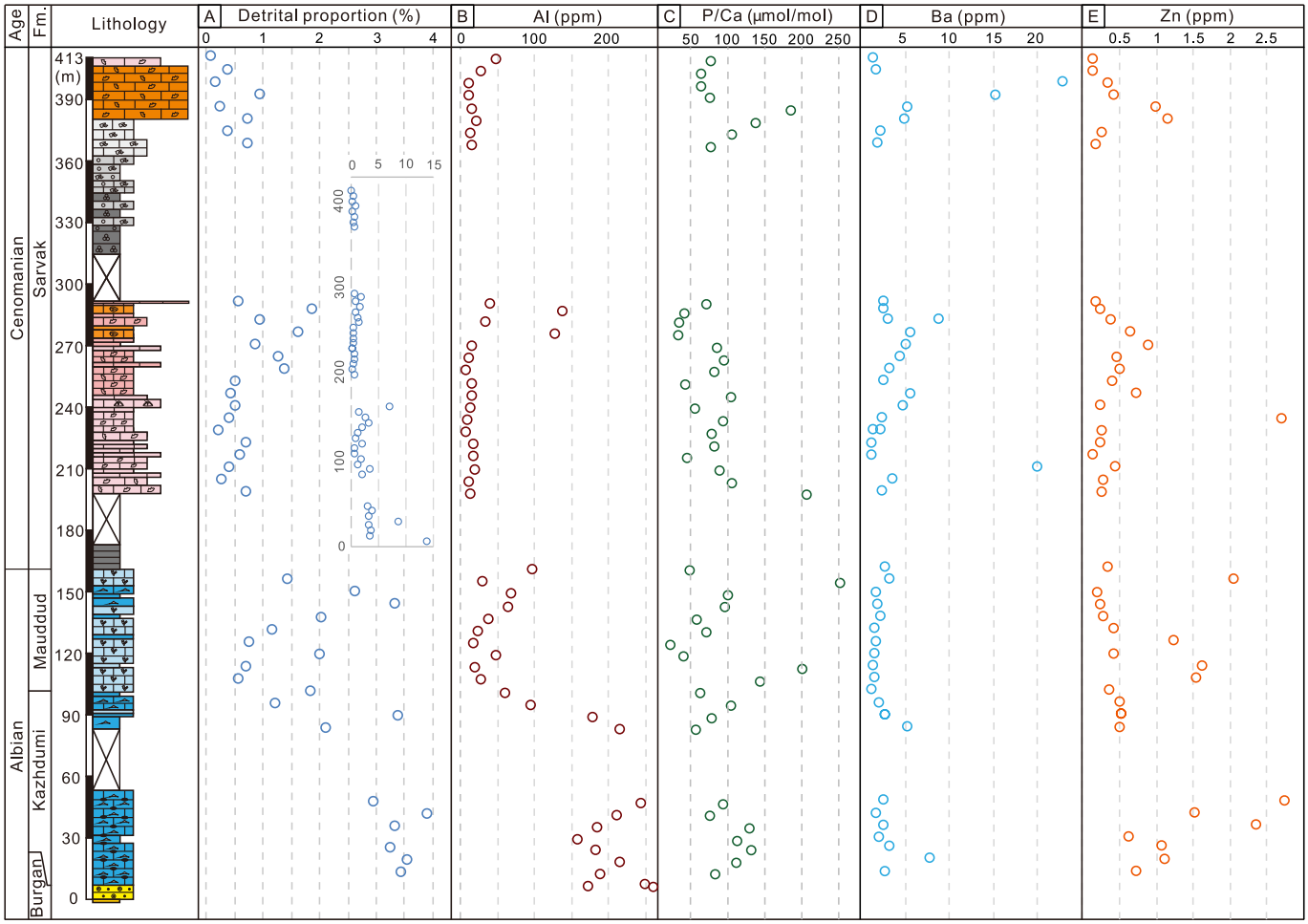

Fig. 8. Khormoj section. (A) Percentage of siliciclastic detritus (all data including off-scale values >5% are shown in rectangular box). (B-E) Concentration of chemical elements. Legend as in Fig. 6. See text for discussion (three extreme values at the bottom of measured section were deleted from Fig. c-e respectively, but included Table-S2).

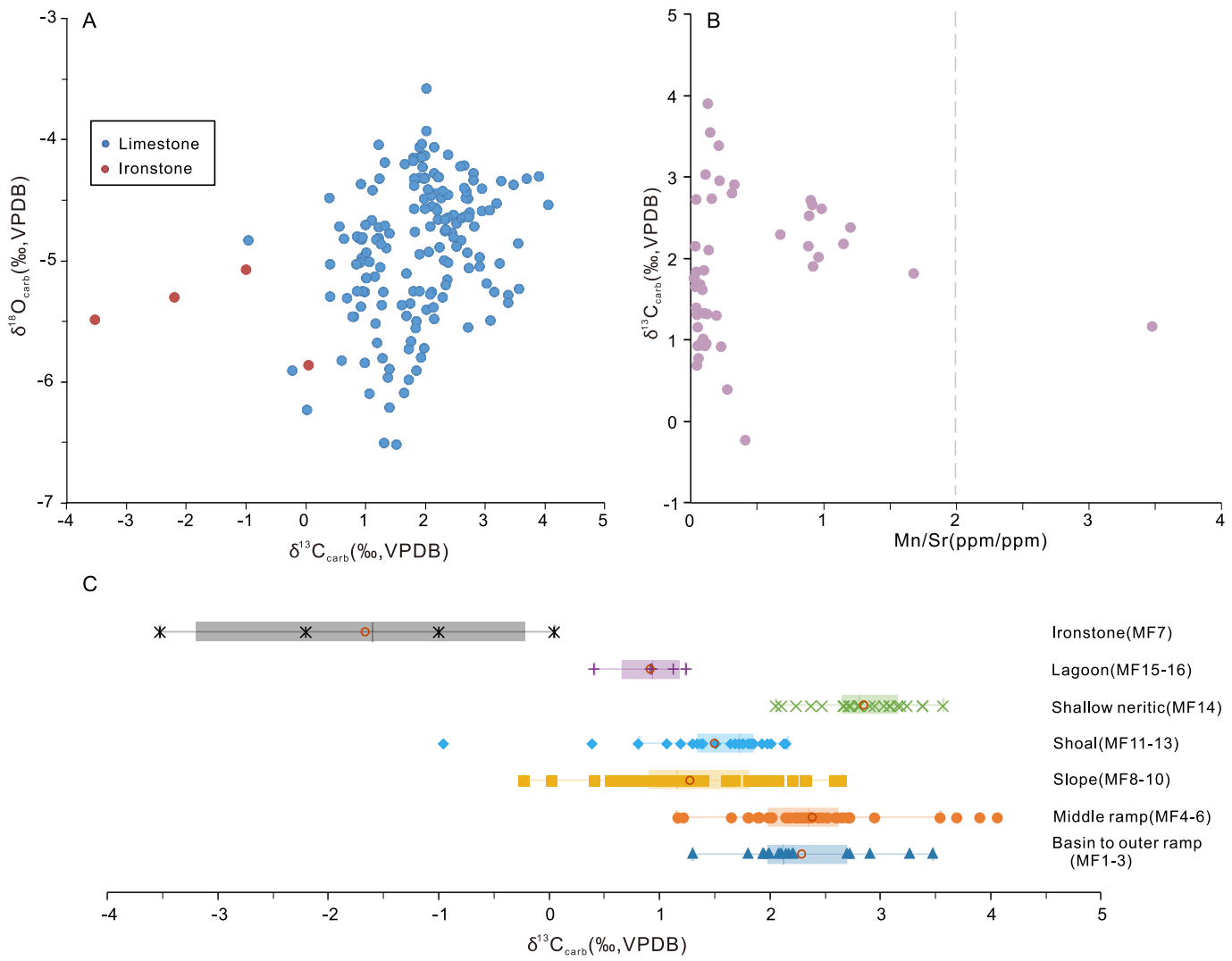

Fig. 9. (A) Cross-plot of $\delta^{13}C$ and $\delta^{18}O$ values. (B) Cross-plot diagram of Mn/Sr and $\delta^{13}C$. Lack of significant covariance and low Mn/Sr indicates no significant diagenetic alteration of stable-isotope values in Khormoj carbonates. (C) Range of $\delta^{13}C$ values from different sedimentary facies of Khormoj section showing lack of correlation with depositional environment.

drowned. The overlying basin to slope sediments (MF2–3) eventually shallow-upward again to rudist shoals (MF10, Fig. 6).

High-resolution microfacies analysis documents two different phases and depositional styles of carbonate-platform development in the Albian and in the Cenomanian. The Kazhdumi Formation, dominated by microfacies MF4 to MF7, was mainly deposited in open-marine environments, whereas the Mauddud Formation, dominated by microfacies MF14, was largely deposited in a shallow neritic sea (Fig.7A). The transition from the Kazhdumi Formation to the Mauddud Formation thus documents a long-term Albian shallowing-upward sequence, as expected in the case of carbonate ramps characterized by a regular depth profile lacking a sharp slope break (Burchette and Wright, 1992). In agreement with previous studies (Vincent et al., 2015), we conclude that the Kazhdumi and Mauddud formations testify to the development of a carbonate ramp, largely consisting of middle ramp and inner ramp sediments, respectively (Fig.7A).

The Sarvak Formation has been considered either a rimmed platform (Razin et al., 2010; Vincent et al., 2015) or a ramp (Ghabeishavi et al., 2010; Mehrabi and Rahimpour-Bonab, 2014; Esrafili-Dizaji et al., 2015; Rikhtegarzadeh et al., 2017; Mohajer et al., 2022). In the Khormoj section, however, the Sarvak Formation displays a topographic profile very different from the Kazhdumi Formation, including a deep-water basin, a slope, a shoal, and a shallow lagoon. Microfacies MF11–12 (shoal) and MF8–10 (slope, Fig.7B) and their spatial relationships indicate that slope sediments were fed from shoals by gravity flows. A slopebreak thus separated the lagoon and shoals from the slope and basin, and field observations clearly document clinoforms downlapping onto basinal deposits (Fig. 2h). In agreement with previous studies (Vincent et al., 2015), the depositional geometry of the Sarvak Formation thus indicates a rimmed platform, with a flat platform top rimmed by rudist shoals (Fig. 7B).

4.4. Stable isotope stratigraphy

In the Kazhdumi and Mauddud formations, $\delta^{13}C$ values display a long-term upsection increase from 1.9‰ to 4.1‰ (Fig. 6). In the Sarvak Formation, $\delta^{13}C$ values decrease slightly from 1.8‰ to 1.1‰ through the lower part, remain stable around 2‰ above, and eventually record a sharp increase to ~3‰ followed by a rapid decrease to 1‰ (Fig. 6). Short-term carbon-isotope excursions (CIE) are also observed through the Khormoj section: CIE1 at the base of the section is a negative spike from 0.05‰ to −3.5‰; CIE2 at the top of the Mauddud Formation is a positive spike with ~1‰ amplitude; CIE 3 in the middle Sarvak Formation consists of two positive spikes with ~0.5‰ and ~ 1‰ amplitude (Fig. 6).

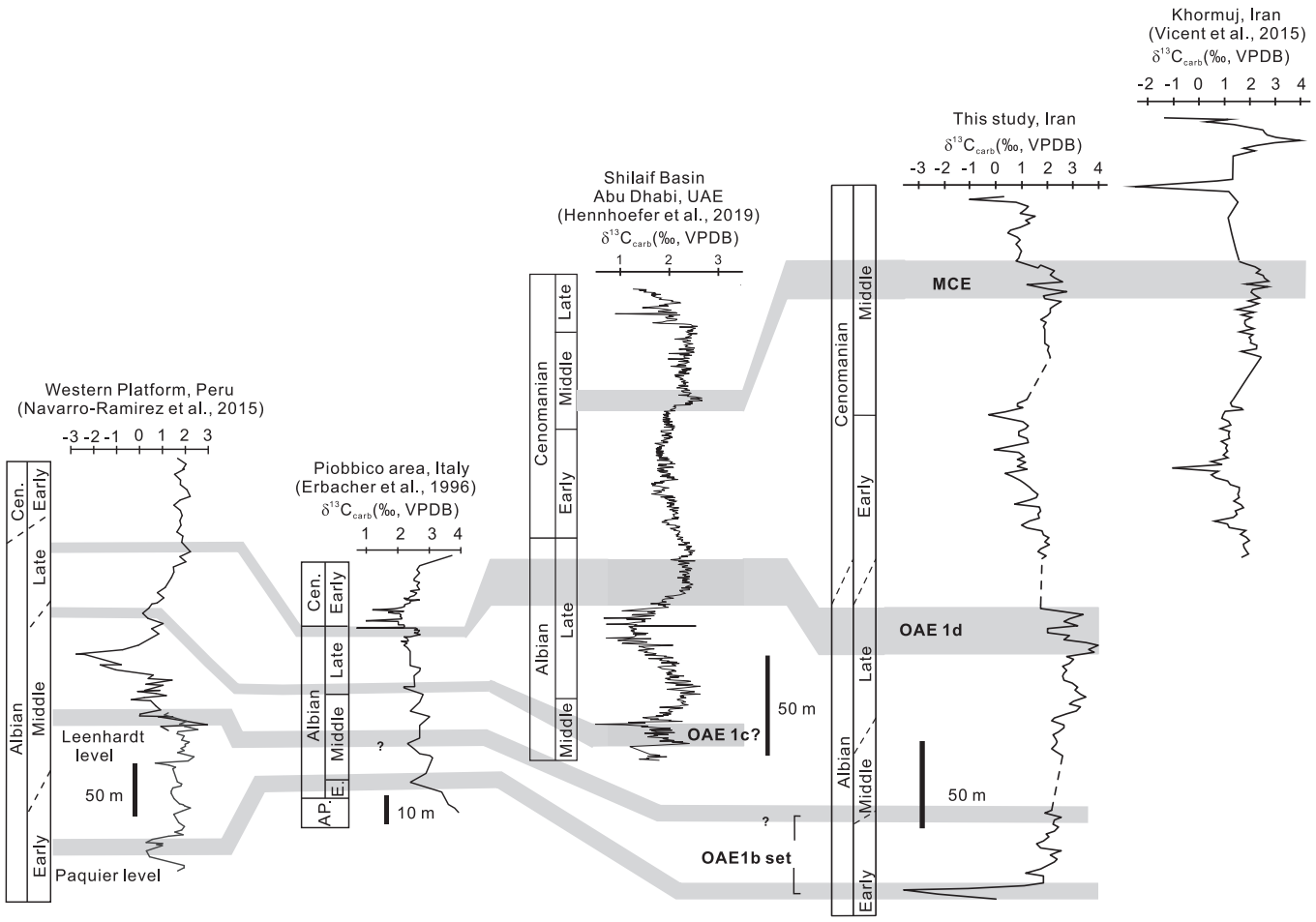

Fig. 10. Correlation of $\delta^{13}C$ curves for Khormoj carbonates (this study and Vincent et al., 2015) with Peru (Navarro-Ramirez et al., 2015), Italy (Erbacher et al., 1996), and United Arab Emirates (Hennhoefer et al., 2019).

4.5. Carbonate geochemistry

The percentage of siliciclastic input in shallow-water carbonate rocks, as calculated from chemical data, reaches maximum values (4%–15%) in the Kazhdumi Formation and decrease to 1.5% in the Mauddud Formation to reach minimum (~0.5%) in the Sarvak Formation (Fig. 8A). Aluminum (Al) follows this trend throughout the Khormoj section (Fig. 8B), whereas nutrient-sensitive elements, such as phosphorus (P/Ca ratio), zinc (Zn), and barium (Ba) show little variation excepting relative high Ba and Zn concentrations in the lower Kazhdumi Formation and upper Sarvak Formation respectively (Fig. 8C-E).

5. Discussion

5.1. Assessment of diagenetic effects on carbon-isotope data

Diagenetic processes can modify the original isotopic composition of marine carbonates, typically resulting in decreased $\delta^{13}C$ and $\delta^{18}O$ values (Banner and Hanson, 1990). The studied carbonate samples from the Khormoj section do not show any evidence of post-depositional dissolution or recrystallization in thin section. Grainstones from the Sarvak Formation do show several generations of carbonate cements (Fig. 5C) but no significant covariance is displayed by the cross-plot of $\delta^{13}C$ and $\delta^{18}O$ values (Fig. 9A). The Mn/Sr ratio in the studied samples is much lower (<1.5) than values generally considered as indicative significantly altered by diagenesis (i.e., > 10; Kaufman and Knoll, 1995) and further evidence against diagenetic effects is the lack of a negative correlation with the carbon isotope curve (Fig. 9B; Jacobsen and Kaufman, 1999).

The isotopic values of the Burgan ironstone ($\delta^{13}C$: ~0 ‰ to ~3.5 ‰, $\delta^{18}O$: −5 ‰ to −6 ‰) are notably lower than limestones for their minerals are siderites (Fig. 9A). The in-situ origin of siderite and their value are within the range of marine environments siderites as summarized by Mozley and Wersin (1992). Therefore, stable-isotope data from the Khormoj section is considered as indicative of the original palaeoceanographic conditions.

5.2. Assessment of facies control on carbon-isotope data

Carbon-isotope values may be influenced also by the presence of different carbonate grains in different facies (Geyman and Maloof, 2021). Carbon isotope values in out ramp-basin (MF1–3) and middle ramp carbonates (MF4–6) are similar and tend to be more negative than for inner ramp carbonates (MF14, Fig.9C). Values in rudist dominated (MF11–13) and slope carbonates (MF8–10) tend to be higher than lagoonal carbonates (MF15–16, Fig.9C). The ironstone (MF7) yielded the lowest $\delta^{13}C$ (Fig.9C). The long-term up-section increase of $\delta^{13}C$ observed in Albian strata may thus partly reflect facies evolution from middle ramp to inner ramp (Fig.6).

Conversely, a lack of correlation between rudist-dominated facies and $\delta^{13}C$ indicate that carbon isotope oscillations during the early to middle Cenomanian are independent of sedimentary facies. Both CIE1 and CIE3 occurred within the same facies (Fig.6). CIE1 shows a negative excursion and back to the normal value within MF7, whereas CIE3 shows a positive excursion in slope environments (MF8–9). CIE2 is a positive $\delta^{13}C$ excursion that occurred during the transition from inner ramp (MF14) to middle ramp (MF3–4) and thus reflects an original

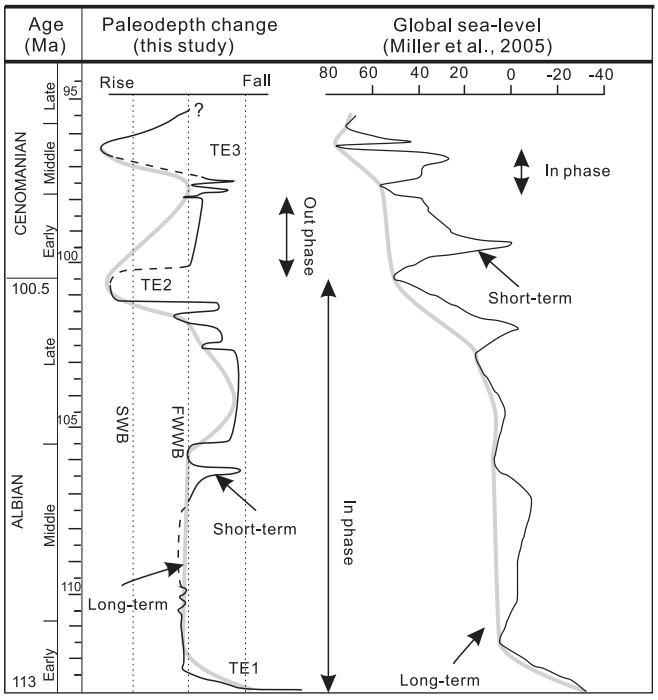

Fig. 11. Comparison between inferred paleowater-depth curve for Khormoj section and eustatic curve of Miller et al. (2005). FWWB: Fair weather wave base, SWB: Storm wave base.

environmental signal rather than facies changes because $\delta^{13}C$ would be expected to decrease from inner to middle ramp carbonates.

5.3. Carbon isotopes and relative sea-level changes

The consistent carbon isotope curve obtained for the Sarvak Formation both by Vincent et al. (2015) and this study shows a long-term decrease from ~2‰ to ~1‰ in the early Cenomanian, followed by a slow increase to ~3‰ in the middle Cenomanian (Fig. 10). The rapid positive shift of carbon isotope related to OAE 2, documented by Vincent et al. (2015), could not be observed in this study because the top of the Sarvak Formation is not exposed in the Khormoj section.

Ammonites (Vincent et al., 2015) and larger benthic foraminifers from the Khormoj section (this study) in the Khormoj section provide biostratigraphic constraints for a worldwide correlation based on $\delta^{13}C$ curves with successions spanning mid-Cretaceous oceanic anoxic events OAE1b, OAE1d, and MCE (Middle Cenomanian Event). The most prominent $\delta^{13}C$ negative excursion (~3.5‰), occurring in the Burgan ironstone at the base of the Kazhdumi Formation, may correlate with the lower Albian Paquier Level of the western Tethys (Fig. 10), one subevent of OAE1b marked by a negative $\delta^{13}C$ excursion (Herrle et al., 2004; Navarro-Ramirez et al., 2015).

The negative excursion by ~0.7‰ observed in the middle part of Kazhdumi Formation may correspond to the Leehhaedt Level (top of OAE1b; Herrle et al., 2004), although discontinuous exposure and poor biostratigraphic control makes such a correlation particular tentative. The prominent positive $\delta^{13}C$ excursion by ~1‰ at the top of the Mauddud Formation dated as late Albian that may be correlate with the latest Albian OAE1d (Yao et al., 2021).

The positive excursion in the upper part of the Sarvak Formation, characterized by two positive peaks (~0.5‰ and ~ 1‰, Fig. 10) and dated as middle Cenomanian, may correlate with the $\delta^{13}C$ excursion also characterized by two positive peaks reported from the western Neo-Tethys realm as a prelude to OAE2 (Andrieu et al., 2015).

Microfacies analysis indicates carbonate deposition in middle ramp environments during the early-middle Albian, following the earliest Albian transgression (TE1). At late middle to early late Albian times, a gradual regression led to deposition on an inner ramp, followed by a major transgressive event and pelagic depositions in the latest Albian (TE2; Fig. 6). Regression in the early Cenomanian led to transition from shoal to lagoonal settings (Fig.6). In the late early Cenomanian, platform drowning during TE3 was followed by a shallowing-upward trend from basin to shoal in the middle Cenomanian (Fig. 6).

Such an inferred long-term paleodepth evolution during the Albian shows some correspondence with global sea-level curve of Miller et al. (2005). Persistent middle ramp deposition after TE1 corresponds to the long-term early to middle Albian eustatic highstand (Fig. 11). The gradual regression followed by TE 2 in the late Albian can well be correlated with the global sea level curve (Fig. 11). However, the regression of the lower part of the Sarvak Formation (after TE2) miscorrelated with eustatic rise during the early Cenomanian (Fig. 11), which may be ascribed to the carbonate platform geometry. Ramps are characterized by notably lower rates of carbonate production than rimmed platforms, which may easily keep-up with sea-level rise (Schlager, 2005; Williams et al., 2011; Sultana et al., 2022). An eustatic rise may thus result in transgression on a slowly accumulating carbonate ramp but on aggradation and even regression on a rapidly growing rimmed platform.

5.4. Response of carbonate factories to siliciclastic influx

Carbonate factories are systems that involve the production of carbonate sediments that is defined by an ecosystem (Schlager, 2005; Pomar and Hallock, 2008; James and Jones, 2016). Documented in this study, two types of shallow-water benthic carbonate factories, dominated by either orbitolinids and green algae (e.g., MF4–6, MF14) in the Kazhdumi and Mauddud formations, or by rudists (MF8–12) with some alveolinids (MF15–17) in the Sarvak Formation. Orbitolinids are one kind of larger benthic foraminifers (LBFs) that mostly live in clear oligotrophic waters (Hallock, 1985), but discoidal orbitolinids, however, can tolerate siliciclastic influx and mesotrophic conditions (Wilmsen, 2000; Pittet et al., 2002; Embry et al., 2010), because better adapt to increased water cloudiness (Hottinger, 1982) or more rapidly respond to a sudden supply of nutrients (Vilas et al., 1995). A positive correlation between the abundance of discoidal orbitolinids and siliciclastic detritus or nutrient levels was observed in lower to middle Cretaceous strata (Vilas et al., 1995; Pittet et al., 2002; Schroeder et al., 2010; Bonvallet et al., 2019).

Rudists are typical Cretaceous reefal fauna grown in siliciclastic-free oligotrophic environments (Sanders and Pons, 1999; van Buchem et al., 2002; Rameil et al., 2010). In the Sarvak Formation exposed in the Khormoj section, rudist debris accumulated in high-energy shoals devoid of siliciclastic influx and favoring efficient recycling of organic matter to nutrients in oligotrophic conditions (Pittet et al., 2002). Orbitolinids are thus replaced by alveolinids which are extreme K-strategists thriving in oligotrophic environments without siliciclastic input (Brasier, 1995; Wilmsen, 2000; Parente et al., 2008).

A similar change in carbonate factories documented in the Barremian-Aptian strata of Arabian plate has been ascribed to siliciclastic influx and changing nutrient levels (van Buchem et al., 2002). Elements behaving as micronutrients (i.e., P/Ca, Ba, Zn) are widely used to indicate nutrient level and paleoproductivity (Tribovillard et al., 2006), but neither of them exhibits a marked change throughout Khormoj section (Figs. 8C-E). This suggests that that nutrient level was not the main control on the observed prominent change in carbonate factories.

In contrast, siliciclastics supply (Fig.8A-B) progressively decreased from the Kazhdumi Formation (4–15% of siliciclastics and 200 ppm Al) to the Mauddud (~2% of siliciclastics and ~ 30 ppm Al) and Sarvak formations (~0.5% of siliciclastics and ~ 15 ppm Al). Observations from both modern and ancient environments indicate that the LBFs are tolerant to siliciclastic influx (Mount, 1984; Coletti et al., 2021).

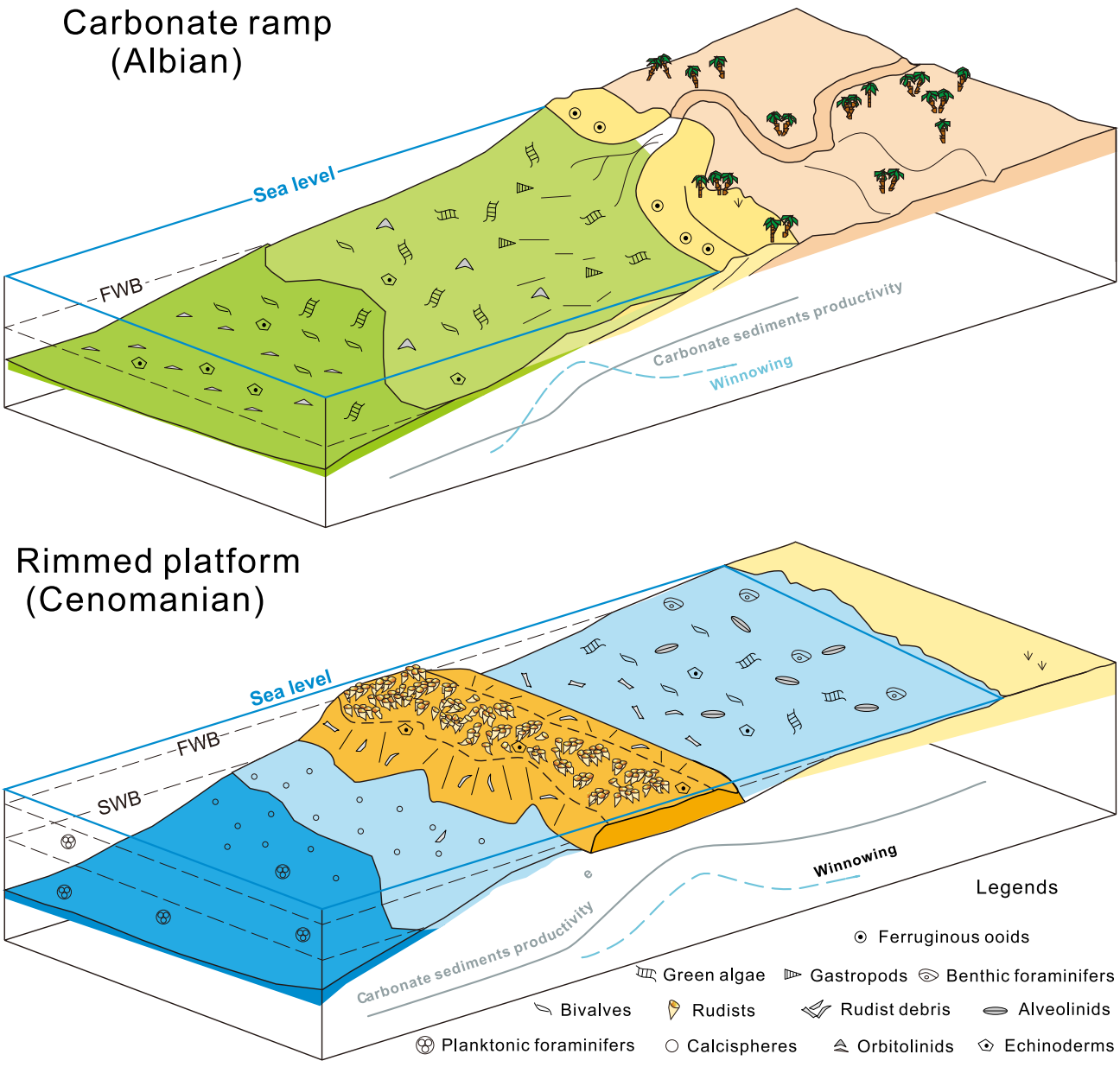

Fig. 12. Two contrasting platform geometries documented in mid-Cretaceous strata of the Khormoj section (Zagros Mountains, Iran): carbonate ramp in the Albian vs. rimmed platform in the Cenomanian (modified from Droste, 2010).

Siliciclastic influx fostered by more humid climate during deposition of the Kazhdumi Formation (Davies et al., 2002; van Buchem et al., 2010, 2011) thus hampered most calcareous biota to thrive in turbid waters, leaving tolerant orbitolinids as the dominant species. Subsequently reduced siliciclastic influx during long-term sea-level rise, led to clearer waters preferred by rudists and alveolinids.

5.5. *Carbonate factories and platform geometry*

The repeated changes in carbonate platform geometry from ramp to rimmed platform documented by Barremian to Cenomanian strata of the Arabian margin have been ascribed to changing rates of carbonate production and accommodation ultimately controlled by short-term sea-level rise (van Buchem et al., 2002; Droste et al., 2010; Razin et al., 2010). During the early transgressive stage of a third-order depositional sequence, balanced carbonate production and generation of new accommodation space may lead to the development of a low-angle ramp. During the late transgressive to early highstand stage, as relative sea-level rises more rapidly, carbonate production may be able to catch up only locally, resulting in the formation of an intrashelf basin rimmed by reefs or shoals (van Buchem et al., 2002, 2011; Droste et al., 2010; Razin et al., 2010; Xu et al., 2022). Our analysis of the Khormoj section makes us question some aspects of this model which predicts that transition from ramp to rimmed platform should rather systematically occur within each third-order depositional sequences. However, six third-order depositional sequences are identified in the Albian to Cenomanian (van Buchem et al., 2011; Vincent et al., 2015) and yet carbonate factories and platform geometry only changed during the earliest Cenomanian (Fig.6).

Moreover, the models assume carbonate-production rate to be a critical factor, leading to formation of a rimmed platform during rapid sea-level rise. This is hardly compatible with what observed in the Khormoj section, where Kazhdumi and Mauddud formations document an inner ramp dominated by green algae (estimated carbonate production rate ~ 0.5 m/kyr; Sultana et al., 2022) and a middle ramp characterized by LBFs and other heterozoans (estimated carbonate

production rate ~ 0.1 m/kyr; Narayan et al., 2021; Sultana et al., 2022). Based on such a contrast in carbonate production rate, the transition from ramp to a rimmed platform with a ~ 90 m-deep basin should occur during any sea-level rise persisting longer than 225 kyr which is however not observed during three different Albian depositional sequence.

Fault activity was also considered as a possible cause of transition from carbonate ramp to rimmed platform (Hughes, 2000; Batt et al., 2008). The study area, however, was situated in a passive margin that did not record any prominent tectonic event before ophiolite obduction in the late Cenomanian (Alavi, 2004).

Our study emphasizes instead the critical role played by siliciclastic influx and by the distinct character of different carbonate factories (Pomar, 2001). A ramp geometry implies a relatively uniform depth distribution of carbonate accumulation, whereas a rimmed platform implies a sigmoidal curve of sediment accumulation (Pomar, 2001; Pomar et al., 2012; Sultana et al., 2022). During the middle to late Albian, the ramp system was dominated by green algae, small benthic foraminifera and orbitolinids. Carbonate production is higher for green algae and small benthic foraminifer than for orbitolinids, but comminuted algal debris is easily transported into deeper environments (Folk and Robles, 1964). Such a resulting homogenization of sedimentation rates from shallower to deeper environments, together with overall low accumulation rates as testified by the occurrence of glaucony in both Kazhdumi and Mauddud formations, favored the ramp geometry (Fig. 12).

During the Cenomanian, orbitolinids were replaced by rudists, capable of a very high carbonate productivity (~24 m/kyr; Steuber, 2000). Rudist tend to shed abundant coarser sand to pebble debris that is readily cemented during early diagenesis (e.g., MF10–12) and thus resists erosion and transport into the basin (Fig. 12). Because pelagic carbonate production is lower by three orders of magnitude (~ 0.03 m/kyr; Einsele, 2000), such a strong difference leads to the formation of a slope break between the platform and the adjacent basin, resulting in the rimmed geometry (Fig. 12).

6. Conclusions

This study integrates new and published sedimentological, biostratigraphic, elemental-geochemistry, and stable-isotope data on mid-Cretaceous carbonate platforms exposed in the Zagros fold-belt of SW Iran. The main conclusions are:

(1) Sixteen carbonate microfacies are recognized in the Albian-Cenomanian stratigraphic succession, documenting basinal, open-marine, delta-front, slope, shoal, shallow-neritic, and lagoonal depositional settings.
(2) By combining field sedimentological evidence and microfacies analysis, two distinct types of carbonate platforms with distinct geometry are identified and described in the studied Khormoj succession: a carbonate ramp dominated by green algae and orbitolinids in the Albian; and a rimmed platform dominated by rudists in the Cenomanian.
(3) These two distinct platform geometries correspond to different benthic carbonate factories which were influenced by the amount of siliciclastic supply, controlled in turn by climate and long-term sea-level rising.
(4) Biostratigraphic and carbon-isotope constraints show that paleodepth changes documented by carbonate microfacies broadly compare with widely accepted long-term eustatic curves for carbonate ramp characterized by lower accumulation rates. Such a correspondence is not observed for rimmed platforms because of a much high productivity that allows their keep-up with sea-level rise.

Declaration of Competing Interest

The authors declare that they have no known competing financial interests or personal relationships that could have appeared to influence the work reported in this paper.

Data availability

No data was used for the research described in the article.

Acknowledgements

We thank Jitao Chen, Marcelle BouDagher-Fadel and Xiaojuan Sun for discussion, Lorenzo Consorti (CNR-ISMAR Trieste) for advice on determination of alveolinid foraminifera. and Haiyan Shen, Miao Lv, and Guang Li for assistance in the laboratory. Two anonymous reviewers and editor Alex Dickson provided valuable comments. This study was financially supported by the National Natural Science Foundation of China (41888101, 42072124, 42072117, 42202118), Open Research Fund of State Key Laboratory of Mineral Deposit Research at Nanjing University (2023-LAMD-K10) and Jiangsu Funding Program for Excellent Postdoctoral Talent.

Appendix A. Supplementary data

Supplementary data to this article can be found online at https://doi.org/10.1016/j.palaeo.2023.111680.

References

Alavi, M., 2004. Regional stratigraphy of the Zagros fold-thrust belt of Iran and its proforeland evolution. Am. J. Sci. 304, 1–20.
Allen, M.B., Armstrong, H.A., 2008. Arabia-Eurasia collision and the forcing of mid-Cenozoic global cooling. Palaeogeogr. Palaeoclimatol. Palaeoecol. 265, 52–58.
Andrieu, S., Brigaud, B., Rabourg, T., Noret, A., 2015. The Mid-Cenomanian Event in shallow marine environments. Influence on carbonate producers and depositional sequences (northern Aquitaine Basin, France). Cretac. Res. 56, 587–607.
Banner, J.L., Hanson, G.N., 1990. Calculation of simultaneous isotopic and trace element variations during water-rock interaction with applications to carbonate diagenesis. Geochim. Cosmochim. Acta 54, 3123–3137.
Batt, L.S., Pope, M.C., Isaacson, E., Montañez, I., Abplanalp, J., Lukasik, J.J., Simo, J.A., 2008. Upper Mississippian Antler foreland basin carbonate and siliciclastic rocks, east-central Idaho and southwestern Montana, U.S.A. distinguishing tectonic and eustatic controls on deposition. In: Lukasik, J.J., Simo, J.A. (Eds.), Controls on Carbonate Platform and Reef Development. SEPM, pp. 147–170. Special Publication 89.
Bonvallet, L., Arnaud-Vanneau, A., Arnaud, H., Adatte, T., Spangenberg, J.E., Stein, M., Godet, A., Follmi, K.B., 2019. Evolution of the Urgonian shallow-water carbonate platform on the Helvetic shelf during the late early cretaceous. Sediment. Geol. 387, 18–56.
Brasier, M.D., 1995. Fossil indicators of nutrient levels. 2. Evolution and extinction in relation to oligotrophy. In: Bosence, D.W.J., Allison, A. (Eds.), Marine Palaeoenvironmental Analysis from Fossils. Geological Society of London, pp. 133–150. Special Publication 83.
Burchette, T., Wright, V.P., 1992. Carbonate ramp depositional systems. Sediment. Geol. 79, 3–57.
Coletti, G., Mariani, L., Garzanti, E., Consani, S., Bosio, G., Vezzoli, G., Hu, X.M., Basso, D., 2021. Skeletal assemblages and terrigenous input in the Eocene carbonate systems of the Nummulitic limestone (NW Europe). Sediment. Geol. 425, 106005.
Davies, R.B., Casey, D.M., Horbury, A.D., Sharland, R., Simmons, M.D., 2002. Early to mid-cretaceous mixed carbonate-clastic shelfal systems. Examples, issues and models from the Arabian Plate. GeoArabia 7, 541–598.
Dunham, R.J., 1962. Classification of carbonate rocks according to depositional textures, in Ham, W.E., ed., Classification of Carbonate Rocks. AAPG Mem. 1, 108–121.
Droste, H., 2010. High-resolution seismic stratigraphy of the Shu'aiba and Natih formations in the Sultanate of Oman. implications for Cretaceous epeiric carbonate platform systems. In: van Buchem, F.S., Gerdes, K.D., Esteban, M. (Eds.), Mesozoic and Cenozoic Carbonate Systems of the Mediterranean and the Middle East. Stratigraphic and Diagenetic Reference Models. Geological Society, London, pp. 187–218. Special Publication 329.
Droste, H., Van Buchem, F., Al-Husseini, M., Maurer, F., 2010. Sequence-stratigraphic framework of the Aptian Shu'aiba Formation in the Sultanate of Oman. In: van Buchem, F., Al-Husseini, M., Maurer, F., Droste, H. (Eds.), Barremian-Aptian Stratigraphy and Hydrocarbon Habitat of the Eastern Arabian Plate. GeoArabia Special Publication 4, pp. 229–283. Special Publication 83.
Einsele, G., 2000. Sedimentary Basins. Evolution, Facies, and Sediment Budget. In: 2nd ed. Springer Science & Business Media, p. 792.

Embry, A.F., Klovan, J.E., 1971. A late Devonian reef tract on Northeastern Banks Island, N.W.T. Bull. Can. Petrol. Geol. 19, 730–781.
Embry, J.C., Vennin, E., Van Buchem, F.S., Schroeder, R., Pierre, C., Aurell, M., 2010. Sequence stratigraphy and carbon isotope stratigraphy of an Aptian mixed carbonate-siliciclastic platform to basin transition (Galve sub-basin, NE Spain). In: van Buchem, F.S., Gerdes, K.D., Esteban, M. (Eds.), Mesozoic and Cenozoic Carbonate Systems of the Mediterranean and the Middle East. Stratigraphic and Diagenetic Reference Models, 329. Geological Society, London, pp. 113–143. Special Publication.
Esrafili-Dizaji, B., Rahimpour-Bonab, H., Mehrabi, H., Kiani-Harchegani, F., Shahverdi, N., 2015. Characterization of rudist-dominated units as potential reservoirs in the middle Cretaceous Sarvak Formation, SW Iran. Facies 61, 14.
Erbacher, J., Thurow, J., Littke, R., 1996. Evolution patterns of radiolaria and organic matter variations. A new approach to identify sea-level changes in mid-cretaceous pelagic environments. Geology 24, 499–502.
Ferrario, F., Mbeck, M.W., Storlazzi, C.D., Fiorenza, M., Shepard, C.C., Airoldi, L., 2014. The effectiveness of coral reefs for coastal hazard risk reduction and adaptation. Nat. Commun. 5, 1–9.
Flügel, E., 2010. Microfacies of Carbonate Rocks. In: Analysis, Interpretation and Application, 2nd ed. Springer-Verlag, Berlin, p. 924.
Folk, R.L., Robles, R., 1964. Carbonate sand of Isla Perez, Alacran Reef complex, Yucatan. J. Geol. 72, 255–292.
Fürsich, F., Alberti, M., Pandey, D., Chaskar, K., Bhosale, S., 2021. Facies analysis and palaeoecology of the Jurassic Spiti Shale Formation in the Spiti area, Northern India. J. Palaeogeogr. 10, 438–462.
Garzanti, E., 1991. Non-carbonate intrabasinal grains in arenites. Their recognition, signifcance, and relationship to eustatic cycles and tectonic setting. J. Sediment. Res. 61, 959–975.
Ge, Y., Lokier, S.W., Hoffmann, R., Pederson, C.L., Neuser, R.D., Immenhauser, A., 2020. Composite micrite envelopes in the lagoon of Abu Dhabi and their application for the recognition of ancient firm-to hardgrounds. Mar. Geol. 423, 106141.
Geyman, E.C., Maloof, A.C., 2021. Facies control on carbonate δ13C on the Great Bahama Bank. Geology 49 (9), 1049–1054.
Ghabeishavi, A., Vaziri-Moghaddam, H., Taheri, A., Taati, F., 2010. Microfacies and depositional environment of the Cenomanian of the Bangestan anticline, SW Iran. J. Asian Earth Sci. 37, 275–285.
Hallock, P., 1985. Why are larger foraminifera large? Paleobiology 11, 195–208.
Hennhoefer, D., Al Suwaidi, A., Bottini, C., Helja, E., Steuber, T., 2019. The Albian to Turonian carbon isotope record from the Shilaif Basin (United Arab Emirates) and its regional and intercontinental correlation. Sedimentology 66, 536–555.
Herrle, J.O., Friedrich, O., Erlenkeuser, H., Hemleben, C., 2004. High-resolution carbon isotope records of the Aptian to lower Albian from SE France and the Mazagan Plateau (DSDP Site 545). a stratigraphic tool for palaeoceanographic and palaeobiologic reconstruction. Earth Planet. Sci. Lett. 218, 149–161.
Homke, S., Vergés, J., Serra-Kiel, J., Bernaola, G., Sharp, I., Garces, M., Goodarzi, M.H., 2009. Late Cretaceous-Paleocene formation of the proto–Zagros foreland basin, Lurestan Province, SW Iran. Geol. Soc. Am. Bull. 121, 963–978.
Hosseini, S., Conrad, M.A., Kindler, P., 2021. Sequence stratigraphy, depositional setting and evolution of the Fahliyan carbonate platform (Zagros fold-thrust belt, SW Iran) in the early cretaceous. Mar. Pet. Geol. 128, 105062.
Hottinger, L., 1982. Larger foraminifera, giant cells with a historical background. Naturwissenschaften 69, 361–371.
Hughes, G.W., 2000. Bioecostratigraphy of the Shu'aiba Formation, Shaybah field, Saudi Arabia. GeoArabia 5, 545–578.
Jacobsen, S.B., Kaufman, A.J., 1999. The Sr, C and O isotopic evolution of Neoproterozoic seawater. Chem. Geol. 161, 37–57.
James, N.P., Jones, B., 2016. In: Origin of Carbonate Rocks. John Wiley and Sons, Chichester, UK, p. 464.
Jones, B., 2010. Warm-water neritic carbonates. In: James, N., Dalrymple, R.W. (Eds.), Facies Models 4. Geological Association of Canada, pp. 341–369.
Kaufman, A.J., Knoll, A.H., 1995. Neoproterozoic variations in the C-isotopic composition of seawater: stratigraphic and biogeochemical implications. Precambrian Res. 73, 27- -49.
Mehrabi, H., Rahimpour-Bonab, H., 2014. Paleoclimate and tectonic controls on the depositional and diagenetic history of the Cenomanian–early Turonian carbonate reservoirs, Dezful Embayment, SW Iran. Facies 60 (1), 147–167.
Mehrabi, H., Esrafili-Dizaji, B., Hajikazemi, E., Noori, B., Mohammad-Rezaei, H., 2019. Reservoir characterization of the Burgan Formation in northwestern Persian Gulf. J. Pet. Sci. Eng. 174, 328–350.
Miller, K.G., Kominz, M.A., Browning, J., Wright, J.D., Mountain, G.S., Katz, M.E., Sugarman, J., Cramer, B.S., Christie-Blick, N., Pekar, S.F., 2005. The Phanerozoic Record of Global Sea-Level Change. Science 310, 1293–1298.
Mount, J.F., 1984. Mixing of siliciclastic and carbonate sediments in shallow shelf environments. Geology 12, 432–435.
Mozley, S., Wersin, P., 1992. Isotopic composition of siderite as an indicator of depositional environment. Geology 20, 817–820.
Mohajer, M.D., Afghah, M., Dehghanian, M., Zakariaii, S.J.S., 2022. Biozonation, microfacies analysis and depositional environment of the Cenomanian sediments (Sarvak Formation) in South Zagros Basin (SW Iran). Carbonates Evaporites 37 (3), 40.
Mutti, M., Hallock, P., 2003. Carbonate systems along nutrient and temperature gradients. Some sedimentological and geochemical constraints. Int. J. Earth Sci. 92, 465–475.
Navarro-Ramirez, J., Bodin, S., Heimhofer, U., Immenhauser, A., 2015. Record of Albian to early Cenomanian environmental perturbation in the eastern sub-equatorial Pacific. Palaeogeogr. Palaeoclimatol. Palaeoecol. 423, 122–137.
Narayan, G.R., Reymond, C.E., Stuhr, M., Doo, S., Schmidt, C., Mann, T., Westphal, H., 2021. Response of large benthic foraminifera to climate and local changes. Implications for future carbonate production. Sedimentology 69, 121–161.
Parente, M., Frijia, G., Di Lucia, M., Jenkyns, H.C., Woodfine, R.G., Baroncini, F., 2008. Stepwise extinction of larger foraminifers at the Cenomanian-Turonian boundary. A shallow-water perspective on nutrient fluctuations during Oceanic Anoxic Event 2 (Bonarelli Event). Geology 36, 715–718.
Pittet, B., Van Buchem, F.S., Hillgärtner, H., Razin, P., Grötsch, J., Droste, H., 2002. Ecological succession, palaeoenvironmental change, and depositional sequences of Barremian-Aptian shallow-water carbonates in northern Oman. Sedimentology 49, 555–581.
Pomar, L., 2001. Types of carbonate platforms, a genetic approach. Basin Res. 13, 313–334.
Pomar, L., Hallock, P., 2008. Carbonate factories: a conundrum in sedimentary geology. Earth Sci. Rev. 87, 134–169.
Pomar, L., Bassant, P., Brandano, M., Ruchonnet, C., Janson, X., 2012. Impact of carbonate producing biotas on platform architecture. Insights from Miocene examples of the Mediterranean region. Earth-Sci. Rev. 113, 186–211.
Pomar, L., Haq, B.U., 2016. Decoding depositional sequences in carbonate systems. Concepts vs experience. Glob. Planet. Chang. 146, 190–225.
Rameil, N., Immenhauser, A., Warrlich, G., Hillgaertner, H., Droste, H.J., 2010. Morphological patterns of Aptian Lithocodium-Bacinella geobodies. Relation to environment and scale. Sedimentology 57, 883–911.
Rikhtegarzadeh, M., Vaziri, S.H., Aleali, M., Bakhtiar, H.A., Jahani, D., 2017. Microbiostratigraphy, microfacies and depositional environment of the Sarvak and Ilam formations in the Gachsaran oilfield, Southwest Iran. Micropaleontology 63 (6), 413–428.
Razin, P., Taati, F., van Buchem, F.S., 2010. Sequence stratigraphy of Cenomanian Turonian carbonate platform margins (Sarvak Formation) in the High Zagros, SW Iran. an outcrop reference model for the Arabian Plate. In: van Buchem, F.S., Gerdes, K.D., Esteban, M. (Eds.), Mesozoic and Cenozoic Carbonate Systems of the Mediterranean and the Middle East. Stratigraphic and Diagenetic Reference Models. Geological Society, London, pp. 187–218. Special Publication 329.
Reijmer, J.J., 2021. Marine carbonate factories. Review and update. Sedimentology 68, 1729–1796.
Sanders, D., Pons, J.M., 1999. Rudist formations in mixed siliciclastic-carbonate depositional environments, Upper cretaceous, Austria. Stratigraphy, sedimentology, and models of development. Palaeogeogr. Palaeoclimatol. Palaeoecol. 148, 249–284.
Saura, E., Garcia-Castellanos, D., Casciello, E., Urruela, A., Verges, J., 2015. Modeling the flexural evolution of the Amiran and Mesopotamian foreland basins of NW Zagros (Iran–Iraq). Tectonics 34, 377–395.
Schlager, W., 2005. Carbonate Sedimentology and Sequence Stratigraphy. SEPM, Concepts in Sedimentology and Paleontology, 200.
Schroeder, R., Neumann, M., 1985. Les grands Foraminifères du Crétacé moyen de la région Méditerranéenne. Geobios Mém. Spécial 7, 1–160.
Schroeder, R., van Buchem, F.S., Cherchi, A., Baghbani, D., Vincent, B., Immenhauser, A. Granier, 2010. Revised orbitolinid biostratigraphic zonation for the Barremian–Aptian of the eastern Arabian Plate and implications for regional stratigraphic correlations. In: van Buchem, F., Al-Husseini, M., Maurer, F., Droste, H. (Eds.), Barremian-Aptian Stratigraphy and Hydrocarbon Habitat of the Eastern Arabian Plate. GeoArabia Special Publication 4, pp. 49–96.
Simmons, M.D., Whittaker, J.E., Jones, R.W., 2000. Orbitolinids from Cretaceous sediments of the Middle East – a revision of the F.R.S. Henson and Associates Collection. In: Hart, M.B., Kaminski, M.A., Smart, C.W. (Eds.), Proceedings of the Fifth International Workshop on Agglutinated Foraminifera. Grzybowski Foundation, pp. 411–437. Special Publication 329.
Steuber, T., 2000. Skeletal growth rates of Upper Cretaceous rudist bivalves. Implications for carbonate production and organism-environment feedbacks. In: Insalaco, E. (Ed.), Carbonate Platform Systems. Components and Interactions. Geological Society, London, pp. 21–32. Special Publication 178.
Sultana, D., Burgess, P., Bosence, D., 2022. How do carbonate factories influence carbonate platform morphology? Exploring production-transport interactions with numerical forward modelling. Sedimentology 68, 1729–1796.
Tribovillard, N., Algeo, T.J., Lyons, T., Riboulleau, A., 2006. Trace metals as paleoredox and paleoproductivity proxies. An update. Chem. Geol. 232, 12–32.
van Buchem, F.S., Pittet, B., Hillgärtner, H., Grötsch, J., Al Mansouri, A.I., Billing, I.M., Droste, H., van Steenwinkel, M., 2002. High-resolution sequence stratigraphic architecture of Barremian/Aptian carbonate systems in northern Oman and the United Arab Emirates (Kharaib and Shu'aiba formations). GeoArabia 7 (3), 461–500.
van Buchem, F.S.P., Baghbani, D., Bulot, L.G., Caron, M., Gaumet, F., Hosseini, A., Kayvani, F., Schroeder, R., Swennen, R., Vedrenne, V., Vincent, B., 2010. Barremian—Lower Albian sequence stratigraphy of southwest Iran (Gadvan, Dariyan and Kazhdumi formations) and its comparison with Oman, Qatar and the United Arab Emirates. In: van Buchem, F.S.P., Al-Husseini, M.I., Maurer, F., Droste, H.J. (Eds.), Barremian- Aptian Stratigraphy and Hydrocarbon Habitat of the Eastern Arabian Plate, GeoArabia Special Publication 4, 2. Gulf PetroLink, Bahrain, pp. 503–548.
van Buchem, F.S.P., Simmons, M.D., Droste, H.J., Davies, R.B., 2011. Late Aptian to Turonian stratigraphy of the eastern Arabian Plate – depositional sequences and lithostratigraphic nomenclature. Pet. Geosci. 17, 211–222.
Vilas, L., Masse, J.P., Arias, C., 1995. Orbitolina episodes in carbonate platform evolution: the early Aptian model from SE Spain. Palaeogeogr. Palaeoclimatol. Palaeoecol. 119, 35–45.
Vincent, B., van Buchem, F.S., Bulot, L.G., Jalali, M., Swennen, R., Hosseini, A.S., Baghbani, D., 2015. Depositional sequences, diagenesis and structural control of the

Albian to Turonian carbonate platform systems in coastal Fars (SW Iran). Mar. Pet. Geol. 63, 46–67.
Williams, H.D., Burgess, M., Wright, P., Della Porta, G., Granjeon, D., 2011. Investigating carbonate platform types. Multiple controls and a continuum of geometries. J. Sediment. Res. 81, 18–37.
Wilmsen, M., 2000. Evolution and demise of a mid-cretaceous carbonate shelf. The Altamira Limestones (Cenomanian) of northern Cantabria (Spain). Sediment. Geol. 133, 195–226.
Xu, Y., Hu, X.M., Garzanti, E., BouDagher-Fadel, M., Sun, G.Y., Lai, W., Zhang, S.J., 2022. Mid-cretaceous thick carbonate accumulation in Northern Lhasa (Tibet). Eustatic vs. Tectonic control? Geol. Soc. Am. Bull. 134, 389–404.
Yao, H., Chen, X., Yin, R., Grasby, S.E., Weissert, H., Gu, X., Wang, C.S., 2021. Mercury evidence of intense volcanism preceded oceanic anoxic event 1d. Geophys. Res. Lett. 48, e2020GL091508.
Ziegler, M.A., 2001. Late Permian to Holocene Paleofacies Evolution of the. Arabian Plate and its Hydrocarbon Occurrences. GeoArabia 6, 445–504.